Available online at www.sciencedirect.com
SCIENCE DIRECT®

Journal of Volcanology and Geothermal Research 154 (2006) 222–236

Journal of volcanology and geothermal research

www.elsevier.com/locate/jvolgeores

Facies variation of eruption units produced by the passage of single pyroclastic surge currents, Hopi Buttes volcanic field, USA

Jorge A. Vazquez [a,*], Michael H. Ort [b]

[a] Department of Geological Sciences, California State University, Northridge, California 91330, USA
[b] Departments of Environmental Sciences and Geology, PO Box 4099, Northern Arizona University, Flagstaff, Arizona 86011, USA

Received 9 October 2005; received in revised form 20 January 2006; accepted 27 January 2006
Available online 24 March 2006

Abstract

Base surges are a significant volcanic hazard associated with phreatomagmatism, but their transport and depositional dynamics are incompletely understood. Stratigraphic analysis and lateral tracing of surge eruption units produced by the passage of single base surges from Haskie tuff ring, Hopi Buttes volcanic field, USA, extend to >1 km from the vent and show similar downcurrent changes in lithofacies. Within 200 m of the vent, eruption units are primarily disorganized lapilli-tuff that is rich in juvenile pyroclasts. At distances ≥200 m from the vent, eruption units transform into a couplet of juvenile-rich lapilli that grades upward into bedform-bearing ash tuff. At distances ≥900 m, upper and lower beds of the eruption unit couplet transform into planar-stratified beds. At distances ≥1100 m, couplets composing different eruption units are almost entirely composed of planar beds and amalgamate to form almost identical planar-bedded ash tuff. The collapse of dense eruption columns following explosive magma-wet sediment interaction generated turbulent surge currents. As the surges traveled away from the Haskie vent, they expanded and partitioned into a basal juvenile-rich traction carpet and overlying accidental-rich ash cloud surge. Near the limit of their runout, the surges cooled and lost their pyroclastic load, leaving planar beds of accidental-rich ash. The deposition of multiple surge eruption units with similar lateral and vertical facies transitions and a paucity of interbedded fallout suggests an eruption characterized by recurring phreatomagmatic explosions of similar size and the generation of surges with similar flow characteristics.

Keywords: base surge; maars; pyroclastic density current; phreatomagmatism; pyroclastic rocks

1. Introduction

Over the past four decades, field studies and eye-witness accounts of historic eruptions have established that dilute pyroclastic density currents, or surges, are a significant volcanic hazard associated with nearly all types of volcanoes and magma compositions (e.g. Moore, 1967; Waters and Fisher, 1971; Sigurdsson et al., 1987). One surge type, base surge, is produced by the collapse of eruption columns during magmatic eruptions (e.g., Belousov et al., 2002; Formenti et al., 2003; Cioni et al., 2003) and especially during phreatomagmatic eruptions formed by explosive interaction between magma and groundwater, surface water, or wet sediment (e.g., Moore, 1967; Waters and Fisher, 1971). Base-surges are commonly generated during the phreatomagmatic eruption of maar and tuff-ring volcanoes (Fisher and Waters, 1970; Wohletz and Sheridan, 1983), and the importance of understanding their characteristics and dynamics is underscored by deadly phreatomagmatic eruptions and their hazard to

* Corresponding author. Tel.: +1 818 677 2564.
E-mail address: jvazquez@csun.edu (J.A. Vazquez).

0377-0273/$ - see front matter © 2006 Elsevier B.V. All rights reserved.
doi:10.1016/j.jvolgeores.2006.01.003

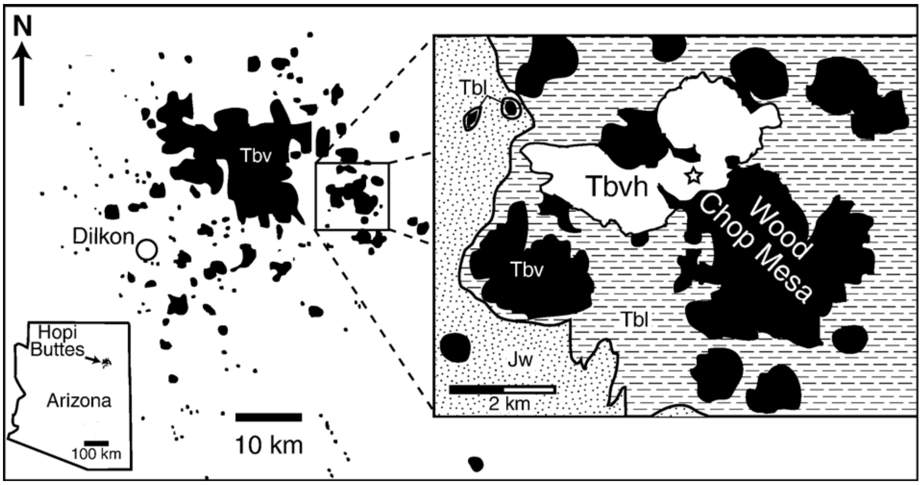

Fig. 1. Location of Hopi Buttes volcanic field and Haskie volcano in northeastern Arizona, USA. Inset shows general geology of Wood Chop Mesa and distribution of deposits from Haskie volcano. Listed units are: Jw, Jurassic Wingate Formation sandstone; Tbl, Lower Member of Bidahochi Formation (mainly mudstones); Tbv, Tertiary volcanic rocks of Hopi Buttes; Tbvh, tuff and lavas from Haskie volcano, star shows center of vent. Adapted from Akers et al. (1971) and Vazquez (1999).

numerous populated areas (e.g. Moore et al., 1966; Crandell, 1975; Johnston et al., 1997). However, despite numerous studies, the controls and dynamics of surge generation and emplacement are incompletely understood (Wohletz, 1998; Valentine and Fisher, 2000).

The dynamics of surge currents have been inferred from numerous studies of pyroclastic deposits. Unfortunately, many surge deposits are poorly exposed or discontinuous. Nevertheless, detailed observations and facies analyses of surge deposits have led to two general models of surge emplacement: (1) an initially expanded, dilute, and turbulent surge that progressively "deflates" downcurrent as it loses energy (Wohletz and Sheridan, 1979), and (2) an initially tephra-laden surge that drops much of its pyroclast load close to its vent and becomes

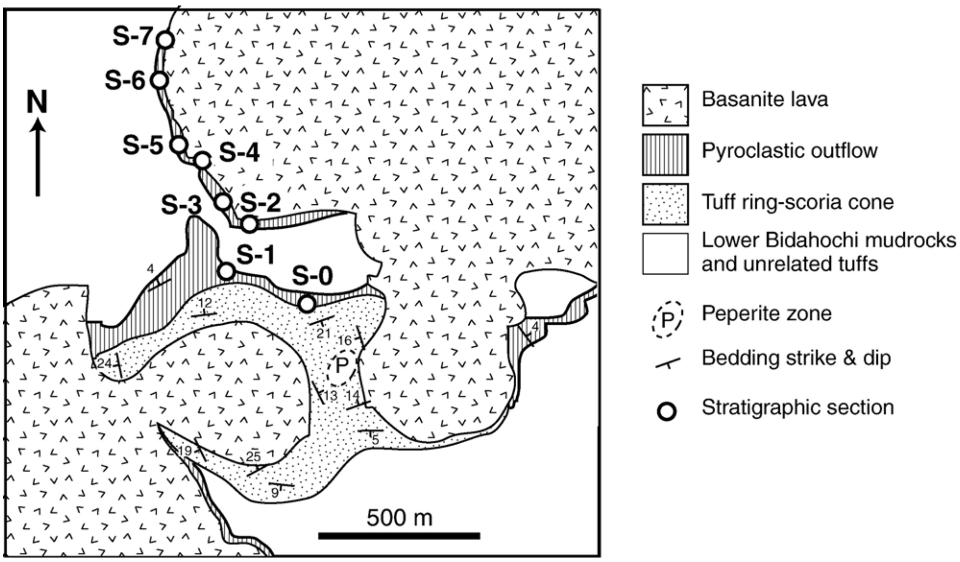

Fig. 2. Simplified geologic map of Haskie volcano showing distribution of pyroclastic outflow deposits around a central vent area composed of tuff ring, scoria cone, and lava lake deposits. The inferred vent area during phreatomagmatism and emplacement of the outflow is delimited by quaquaversally dipping tuff breccia and a zone of peperite intrusion. Two lobes of basanitic lava cap the outflow sequence and preserve a continuous stratigraphy for >1 km north of the vent along low mesa cliffs. Open circles identify the locations and designations of the stratigraphic sections used for facies analysis.

expanded and more dilute downcurrent (Sohn and Chough, 1989; Chough and Sohn, 1990). The discrepancy between these models might reflect differences in the grouping and discrimination of surge-derived beds that may or may not have been deposited by a single passing surge (Wohletz, 1998; Valentine and Fisher, 2000). Few studies recognize or report eruption units produced by the passage of single surges, and those studies that do (e.g., Lajoie et al., 1992; Allen et al., 1996; Colella and Hiscott, 1997; Dellino et al., 2004) are limited by discontinuous exposures, so they are not able to fully document the facies successions for the deposits from individual surge currents. In order to better understand how single base-surge currents evolve as they travel away from their vents, we describe the lateral and vertical facies characteristics of eruption units produced during the eruption of a monogenetic tuff ring in the Hopi Buttes volcanic field, Navajo Nation, Arizona, USA. Lateral and vertical lithofacies progressions of individual surge eruption units indicate progressive downcurrent transformations of surges in response to dilution, increased turbulence and decoupling of pyroclasts from the dilute current. Our conclusions and observations build on previous facies models for surges and serve as a guide for recognizing eruption units in other volcanic areas.

2. Hopi Buttes volcanic field

The Hopi Buttes is a late-Tertiary (8 to 6.5 Ma, and possibly as young as 4 Ma; Damon and Spencer, 2001) mafic volcanic field covering ~800 km^2 of the Colorado Plateau in northeastern Arizona (Williams, 1936; Shoemaker et al., 1962; White, 1991). Hopi Buttes

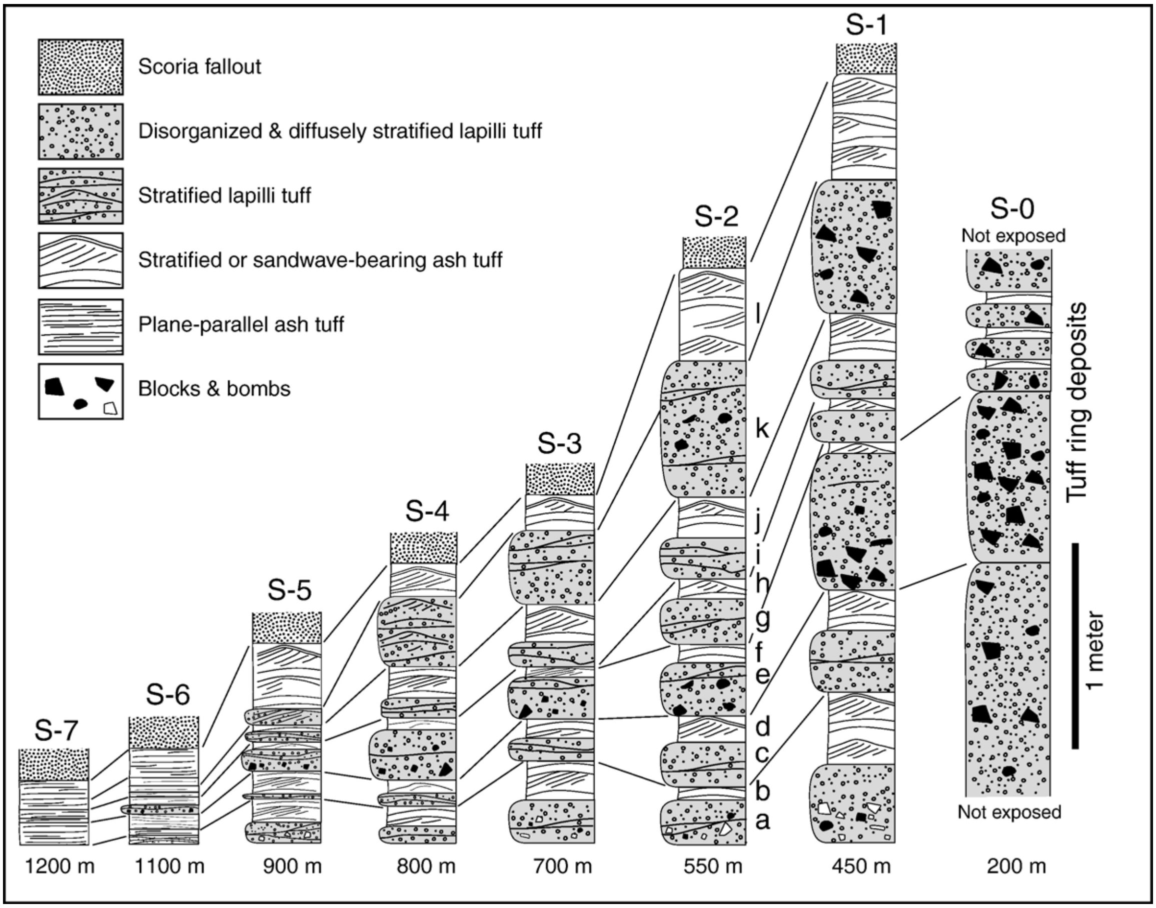

Fig. 3. Stratigraphic sections (locations shown in Fig. 2) and correlated beds of the outflow sequence showing eruption unit couplets and downcurrent successions of lithofacies. Shaded beds represent lithofacies with >40% juvenile lapilli whereas unshaded beds represent lithofacies with <40% juvenile lapilli. Lithofacies groups (discussed in text) are represented by different fill patterns. The outflow is capped by scoria fallout (thickness partly shown) and basanite lava (not shown). Beds representing individual eruption unit couplets referred to in the text (e.g., 2C/2D) are designated in section S-2 by different letters (a through i).

magmas range from basanitic and nephelinitic to lamprophyric in composition (Williams, 1936; Wenrich and Mascarenas, 1982; Vazquez, 1998; Hooten and Ort, 2002). Nearly all Hopi Buttes volcanoes developed through an early phreatomagmatic eruptive phase and by a late magmatic stage of scoria cone construction and effusion of lava (White, 1991; Ort et al., 1998). Phreatomagmatism at Hopi Buttes reflects volcanism in a lacustrine-playa environment (White, 1991). Ascending magma explosively mixed with water-saturated muds and volcaniclastic sediments of the Miocene Bidahochi Formation resulting in phreatomagmatic explosions and the development of over 300 maar-tuff ring volcanoes (White, 1991). In areas of high erosion, the subvolcanic roots of individual Hopi Buttes volcanoes are exposed as diatremes composed of dikes,

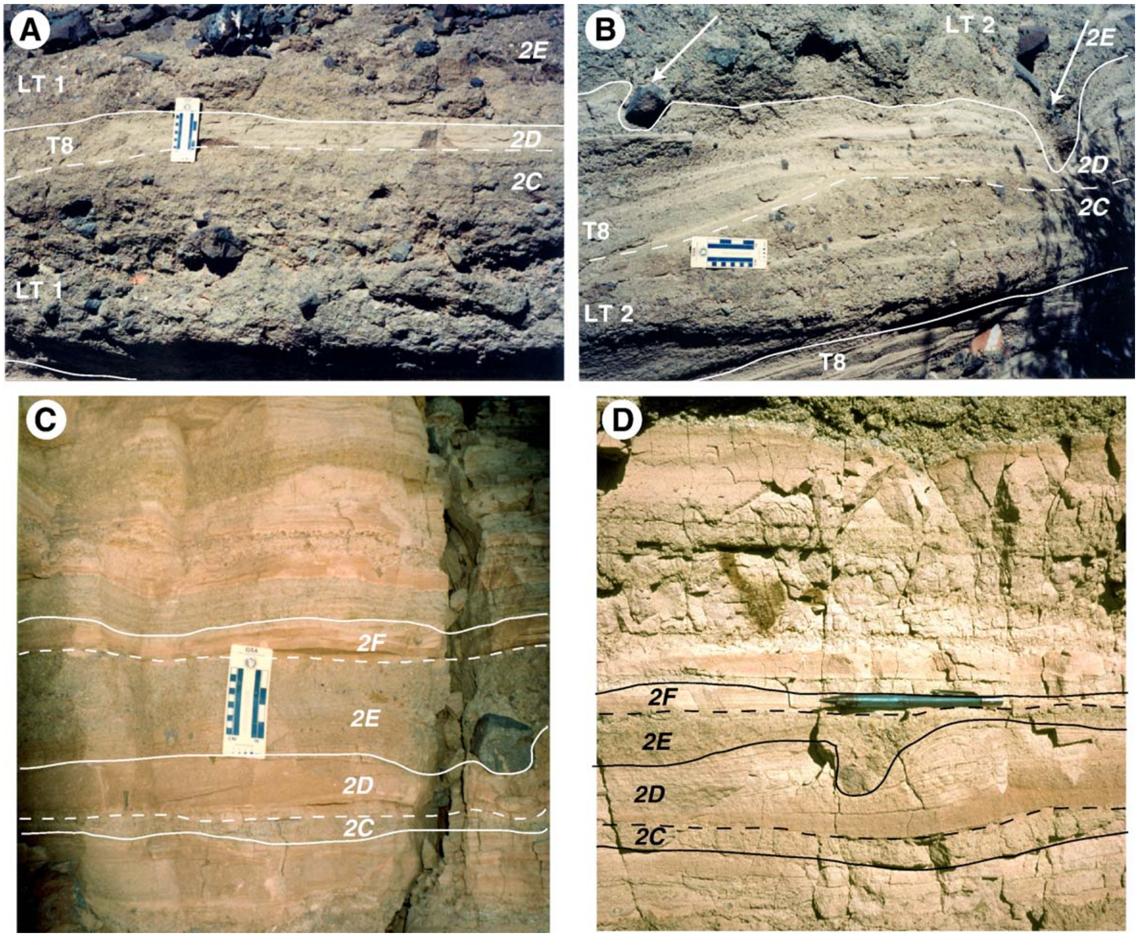

Fig. 4. Photos showing downcurrent lithofacies change for single eruption units from Haskie volcano. In each photo, the surge current traveled from right to left. A. Eruption unit couplet composed of beds C and D in section S-2 (eruption unit 2C/2D; Fig. 3) at ~300 m from vent center. Solid white line delimits upper and lower contacts of the couplet, and dashed line delimits gradational contact between couplet beds. The lower bed is disorganized to diffusely stratified lapilli tuff facies (LT1) and the overlying bed is accidental-rich ash tuff facies (T8). The dark color of the lower bed reflects a high proportion of juvenile pyroclasts whereas the light-color of the overlying bed reflects the high concentration of accidental mud and quartz sand derived from comminuted wallrock mudstone and sandstone. The longest dark increment on the scale is 1 dm. B. Eruption unit 2C/2D at ~450 m from the vent center showing an increased proportion of accidental-rich ash tuff and the appearance of internal ash laminae within the lower bed of dark lapilli tuff. Arrows show impact sags from ballistic blocks. Note the sharing of ash laminae between upper and lower beds of the couplet. C. Outflow sequence at about 850 m from the vent showing partitioning of eruption units into distinct beds of accidental-rich ash (tan) and juvenile-rich lapilli and ash (grey-green). At this distance, the upper ash bed of each couplet is increasingly planar in character and contains local concentrations of accretionary lapilli. D. Exposure of outflow sequence at 1200 m from vent showing the dominance of planar-stratified facies beds at distal locations. In single eruption unit couplets, the upper accidental-rich bed contains subtle bedforms and low-angle truncations of internal laminae, as well as soft-sediment deformation. At this distance, the basal juvenile-rich bed has graded into an ash bed containing a greater proportion of accidental pyroclasts and with subtle planar stratification. Pencil in photo is 14 cm long. (For interpretation of the references to colour in this figure legend, the reader is referred to the web version of this article.)

Table 1
Description and interpretation of Haskie outflow facies

Facies	Pyroclasts	Stratification	Other structures and successions	Interpretation of facies
LT1	Green colored, fine- to medium-grained, poorly orted ash-poor lapilli tuff with scattered coarse-grained lapilli and small blocks. >40% matrix-supported juvenile lapilli. Abundant ballistic blocks and bombs.	Single beds with no or diffuse stratification; stratification is defined by grain-supported lapilli trains and alignment of elongate pyroclasts. Flat upper contacts and undulating lower contacts that truncate underlying beds. Bed thickness averages 25 cm and thickens in substrate lows.	Overall structureless beds in near-vent locations that grade into beds with basal reverse grading. Reverse grading also within lapilli trains. Basal portions of beds contain bombs and blocks with impact sags, whereas middle portions contain blocks resting on their sides. Lags of coarser-grained lapilli is in lows of impact sags.	Formed by rapid sedimentation from high-concentration, turbulent pyroclastic current close to erupting vent (cf. Waters and Fisher, 1971; Fisher and Schmincke, 1984; Lowe, 1988; Branney and Kokelaar, 2002). Development of reverse grading, clast alignment/grading with distance from vent results from downcurrent transformation as surge begins to move away from vent. Unsteady aggradation produces internal lapilli trains (Sohn, 1997) and the high pyroclast concentration in the laterally moving current helps suspend and align entrained blocks and bombs.
LT2	Green colored, medium-grained, and poorly sorted lapilli tuff. >40% juvenile blocky pyroclasts. Abundant blocks and bombs.	Framework-supported lapilli trains and distinctive internal stratification defined by intercalated tan ash laminae with an average thickness of 0.5 cm. Ash laminae are wispy and discontinuous. Upper contacts are generally flat, and bottom contacts are undulatory with local truncation of underlying beds.	Reverse-grading in basal few centimeters of beds and normal grading at upper bounds of beds. Beds contain diffuse sandwaves, downcurrent alignment of lapilli, and lapilli trains with reverse grading. Intercalated ash laminae form sandwaves over irregularities and truncate other bedforms. Ash-rich sandwaves are well developed at >1 km from the vent.	Produced by an unsteady and density-stratified surge current. Upper flat contacts, reverse grading, and imbrication, suggest moderate- to high pyroclast concentrations (Fisher and Schmincke, 1984). However, diffuse internal bedforms suggest pyroclast concentrations were sufficiently dilute for traction sedimentation (Middleton and Southard, 1977) and intercalated ash laminae/bedforms suggest pulsing of the surge current (Sohn, 1997; Branney and Kokelaar, 2002).
LT3	Green colored, medium-grained, and poorly sorted lapilli tuff. >40% juvenile pyroclasts.	Contain intercalated and discontinuous ash laminae (<1 cm thickness) that bifurcate over lows and rejoin over highs.	Reverse-grading in basal few centimeters and normal grading for rest of facies. Undulatory upper and lower contacts with incipient sandwaves on the lee-ides of bedforms in underlying beds.	Produced by a moderate-concentration density-stratified surge current. Normal grading in most of the facies suggests pyroclast concentrations less than for facies LT1 and LT2 currents (cf. Lowe, 1982, 1988). Bedforms and bifurcating ash laminae on the lee-sides of obstacles suggest turbulence and gradients in particle concentration and velocity within the surge (cf. Fisher, 1990). Partitioning of the surge into pulses produced intercalated ash laminae (cf. Sohn and Chough, 1989; Branney and Kokelaar, 2002). Beds with undulatory tops, overall normal grading with basal reverse grading suggest density-stratified flow (cf. Valentine, 1987).
LT5	Green colored, matrix- to	Transitional between LT and T	Upper contacts are gradational	Deposited from surge current of

Table 1 (*continued*)

Facies	Pyroclasts	Stratification	Other structures and successions	Interpretation of facies
	framework-supported, moderately sorted, ash- to medium-grained lapilli tuff; much of the ash is accidental mud and silt. Average bed thickness is 4 cm.	facies with basal reverse grading, overall normal grading, and higher concentration of ash. Differs from facies LT3 in stratification or intercalated ash laminae are absent.	with overlying ash tuffs of acies T9. Basal contacts are locally erosive, and load underlying beds. Upper portions are typically composed of matrix-supported fine-grained lapilli to coarse-grained ash, and contain abundant sandwaves with amplitudes up to 3 cm.	overall moderate pyroclast concentration that effectively segregated clasts by size and density. Mixing with ambient air may have enhanced segregation and upward elutriation of ash. Upward concentration of sandwaves suggests upward dilution and traction-sedimentation.
T4	Thin beds of green colored, coarse-grained, moderately sorted, juvenile-rich ash tuffs with intercalated juvenile-poor, tan ash laminae and fine-grained lapilli trains. Average bed thickness is 7 cm.	Stratification by ash laminae and lapilli trains. Upper portions of this facies are poor in lapilli, and rich in ash.	Flat upper contacts and overall normal grading, slight reverse grading is apparent in single ash laminae and thin beds. Ash laminae pinch-and-swell and bound small low-angle truncation surfaces; truncations locally cut underlying beds and laminae, but bounding ash laminae tend to be continuous. Basal contacts follow undulations of underlying beds and are non-erosive.	Facies T4 is the deposit from a moderate- to low-concentration density-stratified current. Faint reverse grading, overall normal grading, flat upper contacts, and non-erosive bases suggest flow unsteadiness and that significant free settling of clasts through a depositional system of low particle concentration (Middleton and Southard, 1977; Chough and Sohn, 1990). Continuous intercalated ash laminae suggest suspended-load sedimentation from internal pulses or waves that became paired or grouped (cf. Allen, 1982; Valentine, 1987; Lowe, 1988). Intercalated truncation surfaces suggest high rates of shear stress during traction sedimentation (Sohn and Chough, 1989) or result from high-energy and non-depositing pulses analogous to U-shaped channels (e.g., Fisher, 1977).
T6	Green colored, moderately sorted, coarse-grained ash tuff with scattered outsized (up to 2 cm) lapilli. Bed thickness averages 3 cm.	Stratification is defined by thin intercalated tan ash laminae that are laterally continuous.	Upper and lower contacts are typically undulatory, with characteristic bed thickening in lows and thinning over highs of underlying beds. Lack of bedforms. Occurs in sections ≥1 km from the vent. Outsized lapilli produce small-scale asymmetric impact sags filled by medium-grained lapilli.	The fine-grained nature of the deposit, undulatory character, and lack of internal bedforms indicate rapid deposition from a dilute, decelerating, low-concentration current. Small-scale impact sags beneath lapilli indicate moist deposition. Continuous ash laminae that vary in thickness in lows and highs suggest rapid suspension sedimentation in a density-stratified surge current that is decelerating (cf. Fisher, 1971; Fisher and Schmincke, 1984). Multiple laminae in single beds suggest pulsing deposition (cf. Chough and Sohn, 1990; Branney and Kokelaar, 2002).
T7	Tan colored, poorly to moderately sorted, fine- to coarse-grained ash tuff. Pyroclast population is	Undulatory stratification defined by discontinuous ash beds, lapilli trains, and sandwaves. Lapilli trains	Vertical succession of decreasing amplitude sandwaves, and lateral succession of decreasing	Deposited from decelerating surge current. Sandwaves indicate traction sedimentation and low particle concentration, and their vertical

(continued on next page)

Table 1 (*continued*)

Facies	Pyroclasts	Stratification	Other structures and successions	Interpretation of facies
T7	<40% juvenile, and dominated by accidental mud and silt pyroclasts, including accidental-rich accretionary lapilli up to 8 mm in size.	comprise fine- to medium-grained, framework-supported pyroclasts that are locally reversely graded.	amplitude sandwaves with greater distance from vent. Sandwaves in main body of bed are truncated by overlying upper sandwaves that form solitary sets with sharp brink points and a capping thin ash bed showing soft-sediment deformation. Accretionary lapilli are locally deformed by adjacent pyroclasts.	succession of decreasing amplitude indicates a decelerating surge (cf. Fisher and Waters, 1970; Schmincke et al., 1973). Vertical succession of lower main body formed by migrating sandwaves in vigorous surge pulses (cf. Sohn and Chough, 1989; Chough and Sohn, 1990). Ash layer above capping upper sandwave set deposited from terminal “mud rain” from co-surge cloud (cf. Houghton and Nairn, 1989). Accretionary lapilli and deformation indicates moist co-surge cloud concentrated with accidental pyroclasts.
T8	Tan colored, poorly to moderately sorted, fine- to medium-grained ash tuff. Less than 40% juvenile pyroclasts, and dominated by accidental mud and silt pyroclasts.	Stratification is defined by ash laminae and fine-grained lapilli trains with undulations and reverse grading. Largest amplitudes are associated with beds in more proximal localities. Capped by a continuous ash mantle.	Bottom contacts are flat and non-erosive, and top contacts are sharp and loaded by overlying beds. Overall normal grading. Abundant soft-sediment deformation. Resembles facies T7, but lacks vertical succession of truncated sandwaves. Sandwaves form solitary sets with largest sandwaves on lee sides of underlying bedforms. Impact sags beneath blocks and outsized lapilli. Beds and laminae “plaster” or mantle internal structures.	Deposition from a dilute and moist surge current. Internal laminae and reversely graded lapilli trains suggest pulsing suspension- and traction sedimentation (Chough and Sohn, 1990). Overall, normal grading suggests low particle concentration (Middleton and Southard, 1977). In contrast to facies T7, migrating bedforms did not develop in the surge current. Instead, stationary bedforms developed due to little fluctuation in deposition to transport rates (cf. Allen, 1982). Fallout of suspended ash from upper dilute portion of surge produced capping bed of ash tuff.
T9	Tan colored, moderate to well-sorted, fine- to coarse-grained ash tuff; <40% juvenile pyroclasts. Includes outsized lapilli. Located at distances ≥1 km from the vent.	Planar stratification defined by alternating ash trains and discontinuous beds that are structureless to well-stratified with interlaminated ash. Internal stratification locally cross-cut along low-angle surfaces.	Upper contacts are locally contorted, and associated with small-scale flame structures; lower contacts mantle underlying beds. Ash trains pinch and swell, and are the coarsest-grained stratification component of this facies. Contacts between internal ash beds and laminae are diffuse and indistinct. Impact sags associated with outsized lapilli.	Deposited from a rapidly deflating and wet surge. Repetition of thin, planar beds with paucity of bedforms suggests pulsing and high rate of suspension-sedimentation (e.g., Lowe, 1988). Low-angle truncation surfaces suggest shearing of grain layers over depositional surface (Cas and Wright, 1987), perhaps facilitated by the cohesiveness of moist clay. Water condensation and cohesion of clay enhanced deflation and bed flow.
T11	Tan colored, well-sorted ash tuff beds composed of fine- to coarse-grained ash. Less than 40% juvenile ash. Located in sections >1 km from vent.	Planar stratification defined by a repetition of thin and continuous beds and laminae of fine- to coarse-grained ash. Local low-angle truncation surfaces. Thickness varies from 2 to 15 cm.	Generally structureless beds and laminations with local reverse grading. Ash laminae show lateral pinching and swelling and overlie local low-angle truncation surfaces. Ash trains located within structureless beds that are devoid of ash laminae. Impact sags beneath scattered lapilli and coarse-grained ash.	Resembles facies T9, but contains fewer ash trains and contains laterally continuous ash laminae. Produced by rapid deposition from a dilute, moist, and deflating surge with a depositional system of thin, multiple grain layers.

peperites, and tuff breccias (White, 1991; Hooten and Ort, 2002).

3. Pyroclastic deposits at Haskie volcano

Well-exposed and laterally continuous pyroclastic deposits are exposed at Haskie volcano at Wood Chop Mesa, located in the eastern portion of the Hopi Buttes volcanic field (Fig. 1). Haskie volcano is a ~0.5-km diameter tuff ring capped by remnant scoria cones and lava, with a total eruptive volume of ~0.1 km^3 (Vazquez, 1998). Erosion reveals that the core of Haskie volcano is a bomb- and block-rich tuff breccia that grades into an outward-dipping outflow sequence of pyroclastic deposits surrounding the volcano. A central vent area is defined by exposures of peperite and a quaquaversally dipping tuff ring (Fig. 2). The outflow comprises bedded lapilli- to ash-tuff that mantles paleotopography and is traceable to locations over 1 km from the vent (Fig. 2). Juvenile pyroclasts are basanitic sideromelane and tachylite and range from vesicle-poor and blocky to ragged and scoriaceous. Blocks and bombs are common near and within the tuff ring, with bombs having fluidal or cauliflower shapes. Many juvenile pyroclasts contain small (<1 cm) xenoliths of mudrock. Accidental pyroclasts in the outflow are dominated by (1) sandstone and siltstone fragments of the Jurassic Wingate and/or Moenave Formations and lower Bidahochi Formation mudrock; these are the shallowest formations underlying the eastern portion of the Hopi Buttes (Fig. 1) and (2), a basanite lava that is stratigraphically beneath the Haskie deposits (Vazquez, 1998). Blocks of Wingate/Moenave sandstone in the basal bed of the outflow sequence indicate that initial phreatomagmatic explosions began at depths of ≥100 m below the pre-eruptive surface (Vazquez, 1998). Scoriaceous lapilli fallout and basanitic lava cap the outflow sequence (Fig. 3).

We trace the beds composing the outflow sequence along a continuous cliff exposure that extends greater than 1 km north of the vent, and describe the sequence at eight stratigraphic sections (Figs. 2, 3). The most distal section, 1.2 km from the vent, represents the most distal exposure of the primary outflow sequence; beyond this distance, the sequence is reworked and mixed into underlying tuffaceous mudstone. Centimeter-scale description of the outflow sequence reveals multiple beds of lapilli- and/or ash tuff that are distinct in overall color, pyroclast size and composition (accidental vs. juvenile), composition of accidental pyroclasts, and in their contacts with overlying and underlying beds (Fig. 4). Characteristics that distinguish single pyroclastic beds include populations of juvenile and accidental lapilli and blocks that are distinct in type and proportion, and the occurrence of accretionary lapilli, all of which facilitate complete physical tracing and correlation of single beds.

The outflow sequence contains 10 lithofacies that are based on pyroclast size, juvenile pyroclast content, and sedimentary structures (Table 1), although some beds exhibit transitional characteristics. These lithofacies are used to interpret downcurrent changes in flow and depositional processes. Other outflow sections at Haskie volcano (e.g., southeast of the vent area) have similar facies characteristics, but are not as continuously exposed, and were used to corroborate findings in the main lateral section.

4. Discussion

4.1. Downcurrent changes in single pyroclastic beds

The single beds of the outflow sequence exhibit a systematic change in facies with distance from the vent. Close to the vent (≤200 m), most individual beds of the outflow are indistinct and grade into juvenile-rich lapilli tuff and tuff breccia that composes the tuff ring deposits around the vent. With increasing distance from the vent, individual beds of lapilli tuff transform from the poorly sorted and structureless facies LT1 to the stratified LT2 and LT3 facies that contain smaller pyroclasts, indistinct internal sandwaves, and intercalated laminae of ash. Transitions between these facies are gradual. At distances ≥200 m, a bed of accidental-rich ash tuff (facies T8) containing distinct sandwaves develops above the juvenile-rich beds of facies LT1 and/or LT2, and extends to approximately 900 m from the vent. Facies T8 remains above and in contact with the underlying bed of facies LT1 and/or LT2 bed for hundreds of meters. At distances ≥900 m, facies T8 transforms to planar-stratified facies beds of T9, and facies LT2 transforms to facies LT3 and T4. The planar stratified beds contain considerable soft-sediment deformation. Finally, at distances ≥1100 m from the vent, the underlying lapilli tuff bed and overlying ash-tuff bed become nearly identical in terms of pyroclast size and stratification, and amalgamate to form a single bed or couplet of planar stratified facies (T6, T9, T11).

4.2. Eruption units produced by single passing surges

Beds of the lapilli-tuff facies and the ash-tuff facies form a bipartite facies succession that is repeated throughout the Haskie outflow sequence, especially at distances >200 and <1000 m from the vent. A single succession typically comprises a couplet of dark-colored juvenile-rich lapilli tuff facies overlain by light-colored accidental-rich ash tuff facies (Fig. 4). Beds forming individual couplets are linked by similar pyroclast compositions and complementary physical characteristics. For example, the couplet defined by beds 2A and 2B is distinctly enriched in red and orange accidental sandstone. The couplet composed of beds 2F and 2E is distinctly enriched in accidental blocks and lapilli of the older basanite lava through which the Haskie magma erupted. Contacts between the two beds of each couplet are gradational over several millimeters to centimeters (Fig. 4). The upper and lower contacts of the couplets are sharp and distinct. Couplets are best developed at intermediate distances (400–900 m) from the vent. Based on exposed thickness and geometry, individual couplets have volumes between 1 and 2×10^5 m^3.

A couplet's physical coherence and facies characteristics indicate that each is a bipartite eruption unit formed from a single passing surge density current moving away from the vent. We use the term 'eruption unit' sensu Fisher and Schmincke (1984), meaning deposits left by a distinct type of volcanic activity, such as a pyroclastic surge current. Possibly analogous bipartite deposits are produced by high-density turbidity currents (cf. Lowe, 1982; Tinterri et al., 2003). Similar couplets have been deposited by single surges during modern eruptions. For example, the May 18, 1980, Mount St. Helens blast surge deposited a couplet composed of bedded lapilli pumice overlain by sandwave-rich ash (Fisher, 1990). At Soufriere (Edmonds and Heard, 2005) and El Chichon volcanoes (Sigurdsson et al., 1987), the passage of single surges deposited couplets of lapilli and ash. Studies of other ancient pyroclastic deposits (e.g., Frazzetta et al., 1989; Dellino et al., 2004) recognize similar couplets and interpret them to be the deposits from single density-stratified surges. The geometry of sandwaves within the couplets and the asymmetry of impact sags indicate that the surges traveled northward, parallel to the alignment of the stratigraphic sections. Blocks with impact sags are mostly confined to the base or lower portions of each eruption unit (Fig. 4). Some of these blocks compress pyroclasts from the underlying couplet but others do not, suggesting that bursts of ballistic pyroclasts both presaged and coincided with the passage of individual surge currents.

4.3. Facies successions of surge eruption units

To delimit the vertical and lateral architecture of single eruption units, as well as to reconstruct the dynamics of deposition from their parental surges, the facies (Table 1) are divided into four different groups with similar bed characteristics and major sedimentary structures. The groups are generally comparable to those used by other workers (e.g., Wohletz and Sheridan, 1979; Sohn and Chough, 1989; Chough and Sohn, 1990; Lajoie et al., 1992; Colella and Hiscott, 1997) for their facies-based studies of base-surge deposits from small-volume basaltic and rhyolitic volcanoes. The four facies groups are designated: (1) disorganized to diffusely stratified (LT1), (2) stratified (LT2, LT3, LT5, T4, T6), (3) sandwave-bearing (T7, T8), and (4) plane parallel (T9, T11).

Individual eruption units within the Haskie outflow sequence exhibit similar facies successions with distance from the vent (Table 2), although with a different proportion of each facies group at any point along its extent (Fig. 5). Within 200 m of the vent, each eruption unit is dominated by the disorganized-to-diffusely stratified facies group 1. At distances >200 m from

Table 2
Lateral and vertical facies succession of four surge eruption units as a function of distance (meters) from the Haskie vent center

Eruption unit	S-O 200 m	S-1 450 m	S-2 550 m	S-3 700 m	S-4 800 m	S-5 900 m	S-6 1100 m	S-7 1200 m
2B	LT1	T8	T8	T8	T8	T8	T9	
2A		LT1	LT2	LT2	LT3	LT4		
2D	LT1	T8	T8	T8	T8	T9	T9	T9
2C		LT2	LT2	LT3	LT3	LT5	LT5	T11
2F	LT1	T8	T8	T8	T8	T9	T9	T6
2E		LT1	LT1	LT2	LT2	LT2	LT3	
2J	T8	T8	T8	T8	T8	T8	T9	
2I	LT1	LT1	LT2	LT2	LT2	T4	T4	T11

Locations of stratigraphic sections are illustrated in Fig. 3. Single beds are designated by letters (Fig. 3) and bed couplets composing single eruption units are grouped (e.g., 2A and 2B).

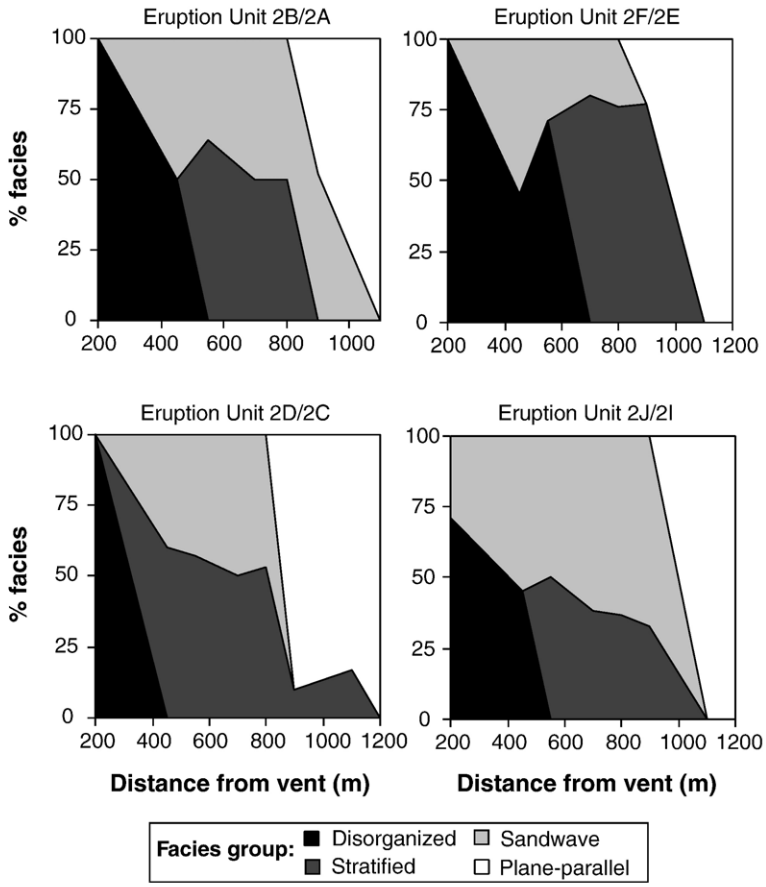

Fig. 5. Proportion of facies groups in four different surge eruption units as a function of distance from the Haskie vent. Facies groups are based on the major physical characteristics of each facies (see text) such as pyroclast size, juvenile content, and sedimentary structures. Each eruption unit shows a downcurrent increase in the proportion of facies containing stratification, with bedforms and sandwaves being best developed at medial distances (400–900 m from vent), and planar stratification dominating deposits at distances of >900 m from the vent.

the vent, ash tuff from sandwave-bearing facies group 3 develops above facies group 1. Between 400 and 600 m from the vent, the disorganized to diffusely stratified facies at the base of each eruption unit transforms into the stratified facies group 2. This vertical succession (stratified facies group overlain by sandwave facies group) is characteristic of eruption units at medial locations (Fig. 5). At distances ≥900 m, the upper portions of eruption units transform from sandwave-facies group to plane-parallel group beds. At distal locations (>1000 m from the vent), the stratified facies group from the lower portions of each eruption unit increasingly transform into the plane-parallel group. At most-distal locations (1200 m), eruption units are entirely composed of the plane parallel facies group (Fig. 5). The downcurrent facies succession for each eruption unit differs from the gross facies occurrence for the entire sequence, reflecting the slightly different runout distances and bed thickness of different eruption units. Hence, the interpretation of how pyroclastic deposits reflect the passing of single currents is more straightforward than using grouped units, as was done in previous studies (e.g., Wohletz and Sheridan, 1979). These vertical and lateral facies transitions within single eruption units suggest that, as single surge currents traveled away from the vent, they transformed through three general stages of transport and sedimentation: (1) an early overladen and diffusely stratified stage, (2) an inflated and density-stratified stage, and (3) a final “deflating” stage when pyroclasts rapidly decouple from the surge current.

4.4. Near-vent deposition of eruption units

Within ~200 m of the crater center, the eruption units reflect the early stages of surge current development. The dominance of disorganized to diffusely stratified facies LT1 (Table 2; Fig. 5) and direct grading of eruption units into the tuff breccia of the tuff ring reflects near-vent accumulation of tephra from collapsing eruption columns and the transformation of some collapses into laterally moving surge currents (Fig. 6). At distances ≥200 m from the vent, early-formed surge currents stratify into a basal carpet that is rich in juvenile lapilli and a dilute and turbulent region that is rich in less-dense accidental ash, and aggrade to form a couplet of lapilli tuff (facies LT1) and ash tuff (facies T8). Stratification of surge currents results from dilution by mixing with ambient air as well as progressive pyroclast sedimentation (Valentine, 1987; Sohn, 1997). Gradational contacts and intercalated ash laminae that cross between the basal carpet and overlying ash tuff (Fig. 4) indicate that some of the accidental-ash rich region was deposited together with the basal carpet. However, the vertical erosional-to-depositional succession of sandwaves in the ash tuff (Table 1; facies T7 and T8) indicates that most of the dilute flow trailed and aggraded behind the basal carpet. A final fall of ash marks the passing of the surge current and produces the continuous bed capping each eruption unit.

4.5. Flow transformation at medial distances

At distances >400 m from the vent, the gradation from disorganized to stratified lapilli tuff within eruption units reflects downcurrent transformation and partitioning of the surge current base (Fig. 6). The appearance of intercalated ash laminae and bedforms in the basal lapilli tuff, together with fluctuations in thickness, indicates that the basal carpet of lapilli and ash becomes diluted and partitioned into pulses. Numerical and theoretical studies (e.g., Valentine, 1987; Sohn and Chough, 1989; Ishimine, 2005) suggest that pulses are likely to develop in turbulent surges, as well as internal waves and vortices that permeate the

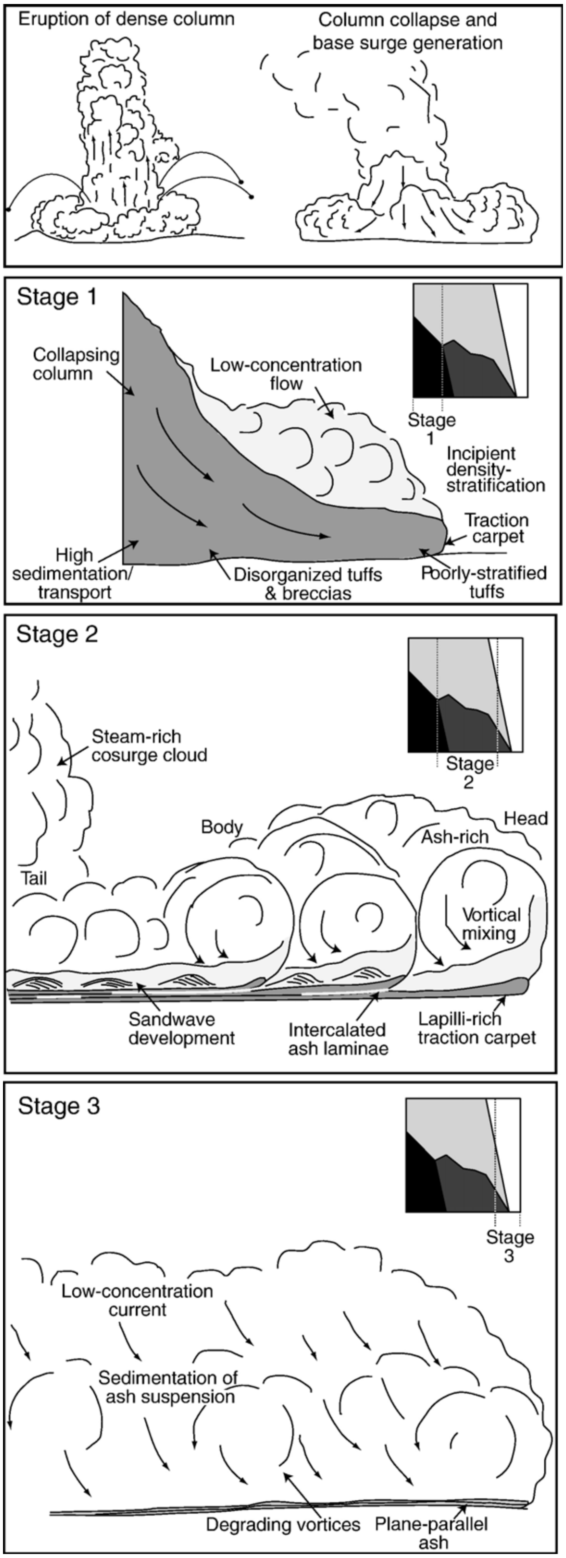

Fig. 6. Cartoon showing development and downcurrent evolution of Haskie surge current in three stages and corresponding eruption unit facies groups. Stage 1: near-vent collapse of phreatomagmatic eruption column and outward movement of a nascent surge. Ballistic blocks fall both ahead and through the surge. As the surge moves away from the vent, it segregates into a basal traction carpet rich in juvenile pyroclasts and an overlying dilute flow rich in less-dense accidental pyroclasts. Stage 2: moving away from the vent zone the surge has thoroughly transformed into a turbulent and density-stratified current and is partitioned into a head, body, and tail region. Internal pulses subdivide the surge and result in overriding between the lapilli-rich traction carpet and its overlying ash-rich flow, producing intercalated ash laminae that splay and are shared between couplet beds (Fig. 4B). Stage 3: at distal locations, suspended pyroclasts above the slowing and increasingly finer grained traction carpet decouple and deposit from a diluted and decelerating current.

surge current as local manifestations and continuous hydraulic structures. Intercalated ash laminae of the basal lapilli tuff bed form as individual pulses aggrade and override fine-grained material deposited just behind the head of the preceding pulse (Fig. 6). As the surge continues to move farther from the vent, preferential settling of dense juvenile pyroclasts and overall dilution yields an increasingly inflated, dilute, and turbulent surge current. Concentration of juvenile pyroclasts in the lower portions of the surge leaves an upper flow that is rich in accidental ash, primarily composed of comminuted sandstone and mudstone that is eventually deposited by saltation and suspension. The vertical succession of truncated sandwaves overlain by single sets of sandwaves and capping ash bed (e.g., facies T7) indicate waning flow and, in turn, that the surge is laterally partitioned into a leading head region, and a slower body, and tail region (Fig. 6). The head of the flow, containing the greatest mass and velocity, deposits most the basal bed of lapilli tuff. Modern surge deposits contain evidence for such lateral partitioning. Base surges from the 1965 maar eruption at Taal volcano, Philippines, plastered pyroclasts against trees, which were finer-grained away from the tree trunks (Moore et al., 1966), suggesting deposition from surges partitioned into a denser head and more dilute and fine-grained tail regions.

4.6. Distal deceleration and decoupling of pyroclasts from the surge current

Distal portions of the outflow sequence reflect final flow transformation of the Haskie surges, with upper and lower beds of eruption units decreasing in mean pyroclast size and grading into beds of plane-parallel ash tuff (Fig. 5). The lower traction-carpet bed remains richest in juvenile pyroclasts but decreases in clast size and transforms into a plane-parallel bed that variably amalgamates with the overlying accidental-rich bed of ash tuff (Fig. 6, Table 2). These plane-parallel beds are generally structureless. However, they contain low-angle truncations and local inverse grading suggesting continuous lateral transport during deposition of tephra as grain layers (e.g., Cas and Wright, 1987). The change from sandwave- to plane parallel beds with concomitant decrease in pyroclast size indicates waning surge energy and decoupling of pyroclasts from the surge current (e.g., Sohn and Chough, 1989; Fisher, 1990). Pronounced impact sags beneath ballistic lapilli and coarse ash, diffuse bed contacts, and local accumulations of accretionary lapilli indicate that the surges became wet as they reached distances of more than 1 km from the vent. Such downcurrent condensation is consistent with progressive cooling of an initially “dry” surge (Koyaguchi and Woods, 1996). This final transformation contributed to deceleration and loss of momentum and the eventual demise of each surge current (Fig. 6).

4.7. Recurring phreatomagmatic explosions and the generation of surges

The similar architecture of the Haskie eruptions units suggests vent explosions that generated surges of similar size, energy, and flow behavior. The eruption units have similar runout distances and their lateral and vertical facies transitions occur within the same narrow zones. In turn, this repetitive generation of self-similar surges suggests a recurring cycle of explosive conditions in the vent conduit that led to eruption column formation and surge-forming column collapse. In general, eruption column collapse and associated surge generation during phreatomagmatism reflects the proportions of magma and water ± sediment and their interaction dynamics, as well as their depth of mixing, near-field hydrogeology, and intrinsic magma properties (Wohletz and Sheridan, 1983; Koyaguchi and Woods, 1996; Sohn, 1996; White, 1996). Diatreme peperites exposed in eroded Hopi Buttes volcanoes indicate that mixing of magma and pore water in Bidahochi mud occurred at near optimum proportions for explosive conversion of water to steam (Hooten and Ort, 2002) as determined by theoretical and experimental studies (e.g., Wohletz, 1983; Zimanowski et al., 1997). The self-similar surges of the outflow sequence suggest that these mixing conditions were repeatedly reached in the Haskie vent. The paucity of fallout between the surge eruption units (Fig. 3) suggests periodic vent explosions and eruption column generation, rather than surge generation from a sustained eruption column (e.g., Talbot et al., 1994). The sharp gradation between phreatomagmatic and magmatic eruption styles recorded in the upper portion of the outflow sequence (Fig. 3) indicates that magma–water interaction ratios increased abruptly in the Haskie vent, resulting in scoria cone formation and final effusion of lava.

Ballistic blocks at the base of several eruption units provide insight into the dynamics and vent pressures associated with phreatomagmatic explosions at Haskie tuff ring. These blocks indent the tops of underlying eruption units and are likely to have landed just before the passage of their associated surges, whereas blocks within the eruption units (Fig. 4) are likely to have fallen into moving surges. Ejection velocities for ballistic

Table 3
Ejection velocities for ballistic blocks from Haskie tuff ring

Eruption unit	Distance from vent (m)	Block diameter (cm)	Initial velocity (m s^{-1}) 45° ejection angle	Initial velocity (m s^{-1}) 65° ejection angle
K/L	500	40	75	89
E/F	450	55	69	81
C/D	550	40	79	94
A/B	700	37	93	112
	800	53	97	116

Velocities calculated using the ballistic calculator from Mastin (2001). Eruption units are the same designated in Fig. 3. Variables for calculations (see Mastin, 2001): no tailwind, cube geometry with a coefficient of drag of 1 (cf. Self et al., 1980) based on the irregular shape of Haskie blocks, block density of 2700 kg/m^3, 1920 m elevation for the eruption, 6.5 °C/km thermal lapse rate, and reduced drag during initial travel through a 100 m region of gas above the vent (cf. Self et al., 1980; Fagents and Wilson, 1993; Mastin, 2001). An actual tailwind of 10 m/s would result in calculated ejection velocities that are too high by 10% (45° angle) to 15% (65° angle).

blocks from the bases of different eruption units range from 70 to 115 m/s for ejection angles of 45° to 65° (Table 3); ejection angles for blocks from maar eruptions are likely to vary yet be within these values (Self et al., 1980). These velocities are comparable to those calculated for ejected blocks from phreatomagmatic explosions at other maars, such as Ukinrek (75–100 m/s; Self et al., 1980; Fagents and Wilson, 1993; Waitt et al., 1995). The similar ejection velocities for blocks beneath different eruption units suggest recurring explosions of similar energy and pressure in the vent, consistent with our findings from the surge deposits. However, velocities associated with blocks beneath the first eruption unit (A/B in Fig. 3) are somewhat greater than the others (Table 3), suggesting that the vent-opening blast, which rooted in Wingate sandstone, was most explosive. At other Hopi Buttes maars, the most powerful phreatomagmatic explosions also rooted in Wingate sandstone and ejected blocks the farthest (White, 1991). Assuming a gas content of 1 to 10 wt.% for the steam–pyroclast mixture formed by explosions in the Haskie vent (e.g., Self et al., 1980; Fagents and Wilson, 1993), the ejection velocities suggest a vent pressure of up to 3 MPa for the vent-opening blast and subsequent explosions with vent pressures of up to 1 MPa (Self et al., 1980; Fagents and Wilson, 1993).

5. Summary and conclusions

Continuously exposed eruption units produced by the passage of single base surges are exposed at Haskie tuff ring, Hopi Buttes volcanic field. Near their source vent, eruption units are composed of juvenile-rich lapilli tuff that grades into the disorganized tuff breccia of the tuff ring. Single eruption units are delimited by a couplet of lapilli- and ash tuff at distances of >400 m from the vent, representing transformation of the surge into a density stratified current. At distances >900 m from the vent, the eruption units grade into beds of plane-parallel ash tuff. This downcurrent facies succession reflects deposition from “dry” surges that became increasingly turbulent and density-stratified as they traveled away from the vent, and subsequently “deflated” as pyroclasts quickly decoupled from the surge current due to deceleration, dilution by ambient air, and condensation of gaseous water. The vertical and lateral facies transitions of single eruption units in the Haskie outflow sequence support models for surges that expand and become dilute as they move away from their vents (e.g., Sohn and Chough, 1989; Chough and Sohn, 1990). At Haskie volcano, collapse of tephra-laden eruption columns produced discrete surge currents, rather than quasi-continuous surges from a sustained and partly collapsing eruption column (e.g., Talbot et al., 1994). The characteristics of the surge eruption units from Haskie volcano may serve as guides for recognizing surge eruption units in modern or ancient deposits of phreatomagmatism.

Acknowledgements

We thank the Haskie family and Navajo Nation for access to their land, and we are grateful to Jason Hooten, Todd Dallegge, and David Blauvelt for able field assistance. We thank P. Dellino and an anonymous referee for their constructive reviews of this paper. Field work on the Navajo Nation was conducted under a permit from the Navajo Nation Minerals Department, and any persons wishing to conduct geologic investigations on the Navajo Nation must first apply for and receive a permit from the Navajo Nation Minerals Department, P.O. Box 1910, Window Rock, Arizona 865115.

References

Akers, J.P., Shorty, J.C., Stevens, P.R., 1971. Hydrogeology of the Cenozoic igneous rocks, Navajo and Hopi Indian Reservations, Arizona, New Mexico, and Utah. U.S. Geological Survey Professional Paper, vol. 521-D.

Allen, J.R.L., 1982. Sedimentary Structures, their Character and Physical Basis. Developments in Sedimentology, vol. 30A–B. Elsevier.

Allen, S.R., Bryner, V.F., Smith, I.E.M., Ballance, P.F., 1996. Facies analysis of pyroclastic deposits within basaltic tuff-rings of the

Auckland volcanic field, New Zealand. New Zealand Journal of Geology and Geophysics 39, 309–327.

Belousov, A., Voight, B., Belousova, M., Petukhin, A., 2002. Pyroclastic surges and flows from the 8–10 May 1997 explosive eruption of Bezymianny volcano, Kamchatka, Russia. Bulletin of Volcanology 64, 455–471.

Branney, M.J., Kokelaar, P., 2002. Pyroclastic density currents and the sedimentation of ignimbrites. Geological Society 27.

Cas, R.A.F., Wright, J.V., 1987. Volcanic Successions: Modern and Ancient. Chapman and Hall.

Chough, S.K., Sohn, Y.K., 1990. Depositional mechanics and sequences of base surges, Songaskan tuff ring, Cheju Island, Korea. Sedimentology 37, 1115–1135.

Cioni, R., Sulpizio, R., Garruccio, N., 2003. Variability of the eruption dynamics during a Subplinian event: the Greenish Pumice eruption of Somma–Vesuvius (Italy). Journal of Volcanology and Geothermal Research 124, 89–114.

Colella, A., Hiscott, R.N., 1997. Pyroclastic surges of the Pleistocene Monte Guardia sequence (Lipari Island, Italy): depositional processes. Sedimentology 44, 47–66.

Crandell, D.R., 1975. Assessment of volcanic risk on the island of Oahu, Hawaii, U.S. Geological Survey Open-File 75–287.

Damon, P.E., Spencer, J.E., 2001. K–Ar geochronologic survey of the Hopi Buttes volcanic field. In: Young, R.A., Spamer, E.E. (Eds.), Colorado River, Origin and Evolution, pp. 53–56.

Dellino, P., Isaia, R., Veneruso, M., 2004. Turbulent boundary layer shear flows as an approximation of base surges at Campi Flegrei (Southern Italy). Journal of Volcanology and Geothermal Research 133, 211–228.

Edmonds, M., Heard, R.A., 2005. Inland-directed base surge generated by the explosive interaction of pyroclastic flows and seawater at Soufriere Hills volcano, Montserrat. Geology 33, 245–248.

Fagents, S.A., Wilson, L., 1993. Explosive volcanic eruptions—VII. The ranges of pyroclasts ejected in transient volcanic explosions. Geophysical Journal International 113, 359–370.

Fisher, R.V., 1971. Features of coarse-grained, high-concentration fluids and their deposits. Journal of Sedimentary Petrology 41, 916–927.

Fisher, R.V., 1977. Erosion by volcanic base-surge density currents: U-shaped channels. Geological Society of America Bulletin 88, 1287–1297.

Fisher, R.V., 1990. Transport and deposition of a pyroclastic surge across an area of high relief: the 18 May 1980 eruption of Mount St. Helens, Washington. Geological Society of America Bulletin 102, 1038–1054.

Fisher, R.V., Schmincke, H.U., 1984. Pyroclastic Rocks. Springer-Verlag, Berlin.

Fisher, R.V., Waters, A.C., 1970. Base surge bed forms in maar volcanoes. American Journal of Science 268, 157–180.

Formenti, Y., Druitt, T.H., Kelfoun, K., 2003. Characterisation of the 1997 Vulcanian explosions of Soufriere Hills Volcano, Montserrat, by video analysis. Bulletin of Volcanology 65, 587–605.

Frazzetta, G., La Volpe, L., Sheridan, M.F., 1989. Interpretation of emplacement units in recent surge deposits on Lipari, Italy. Journal of Volcanology and Geothermal Research 37, 339–350.

Hooten, J.A., Ort, M.H., 2002. Peperite as a record of early-stage phreatomagmatic fragmentation processes: an example from the Hopi Buttes volcanic field, Navajo Nation, Arizona, USA. Journal of Volcanology and Geothermal Research 114, 95–106.

Houghton, B.F., Nairn, I.A., 1989. Phreatomagmatic and strombolian activity at White Island volcano 1976–82: deposits and depositional mechanisms. In: Houghton, B.F., Nairn, I.A. (Eds.), The 1976–82 Eruption Sequence at White Island Volcano (Whakaari), Bay of Plenty, New Zealand. New Zealand Geological Survey Bulletin, vol. 103.

Ishimine, Y., 2005. Numerical study of pyroclastic surges. Journal of Volcanology and Geothermal Research 139, 33–57.

Johnston, D.M., Nairn, I.A., Thordarson, T., Daly, M., 1997. Volcanic impact assessment for the Auckland volcanic field. Auckland Regional Council Technical 79.

Koyaguchi, T., Woods, A.W., 1996. On the formation of eruption columns following explosive mixing of magma and water. Journal of Geophysical Research 101, 5561–5574.

Lajoie, J., Lanzafame, G., Rossi, P.L., Tranne, C.A., 1992. Lateral facies variations in hydromagmatic pyroclastic deposits at Linosa, Italy. Journal of Volcanology and Geothermal Research 54, 135–143.

Lowe, D.R., 1982. Sediment gravity flows: II. Depositional models with special reference to the deposits of high-density turbidity currents. Journal of Sedimentary Petrology 52, 279–297.

Lowe, D.R., 1988. Suspended-load fallout rate as an independent variable in the analysis of current structures. Sedimentology 35, 765–776.

Mastin, L.G., 2001. A Simple Calculator of Ballistic Trajectories for Blocks Ejected during Volcanic Eruptions. US Geological Survey Open-File, vol. 01-45.

Middleton, G.V., Southard, J.B., 1977. Mechanics of Sediment Movement. Society of Economic Paleontologists and Mineralogists Short Course Number 3.

Moore, J.G., 1967. Base surge in recent volcanic eruptions. Bulletin of Volcanology 30, 337–363.

Moore, J.G., Nakamura, K., Alcaraz, A., 1966. The 1965 eruption of Taal volcano. Science 151, 955–960.

Ort, M.H., Dallegge, T.A., Vazquez, J.A., White, J.D.L., 1998. Volcanism and sedimentation in the Mio–Pliocene Bidahochi Formation, Navajo Nation, NE AZ. In: Duebendorfer, E.M. (Ed.), Geologic Excursions in Northern and Central Arizona, pp. 35–57.

Schmincke, H.U., Fisher, R.V., Waters, A.C., 1973. Antidune and chute and pool structures in the base surge deposits of the Laacher See area, Germany. Sedimentology 20, 553–574.

Self, S., Kienle, J., Huot, J.P., 1980. Ukinrek maars, Alaska, II. Deposits and formation of the 1977 craters. Journal of Volcanology and Geothermal Research 7, 39–65.

Shoemaker, E.M., Roach, C.H., Byers Jr., F.M., 1962. Diatremes and uranium deposits in the Hopi Buttes, Arizona. Petrologic Studies; A Volume to Honor A.F. Buddington. Geological Society of America, pp. 327–355.

Sigurdsson, H., Carey, S.N., Fisher, R.V., 1987. The 1982 eruptions of El Chichon volcano, Mexico (3): physical properties of pyroclastic surges. Bulletin of Volcanology 49, 467–488.

Sohn, Y.K., 1996. Hydrovolcanic processes forming basaltic tuff rings and cones on Cheju Island, Korea. Geological Society of America Bulletin 108, 1199–1211.

Sohn, Y.K., 1997. On traction-carpet sedimentation. Journal of Sedimentary Research 67, 502–509.

Sohn, Y.K., Chough, S.K., 1989. Depositional processes of the Suwolbong tuff ring, Cheju Island (Korea). Sedimentology 36, 837–855.

Talbot, J.P., Self, S., Wilson, C.J.N., 1994. Dilute gravity current and rain-flushed deposits in the 1.8 ka Hatepe Plinian deposit, Taupo, New Zealand. Bulletin of Volcanology 56, 538–551.

Tinterri, R., Drago, M., Consonni, A., Davoli, G., Mutti, E., 2003. Modelling subaqueous bipartite sediment gravity flows on the basis of outcrop constraints: first results. Marine and Petroleum Geology 20, 911–933.

Valentine, G.A., 1987. Stratified flow in pyroclastic surges. Bulletin of Volcanology 49, 616–630.
Valentine, G.A., Fisher, R.V., 2000. Pyroclastic surges and blasts. In: Sigurdsson, H., Houghton, B., McNutt, S.R., Rymer, H., Stix, J. (Eds.), Encyclopedia of Volcanoes.
Vazquez, J.A., 1998. Maar volcanism in the Wood Chop Mesa area, Hopi Buttes volcanic field, Navajo Nation, Arizona. MS Thesis, Northern Arizona University.
Vazquez, J.A., 1999. Map of volcanic geology of the Wood Chop Mesa area, Hopi Buttes (Tsezhin Bii), Navajo Nation, Arizona. Arizona Geological Survey Map CM-99-A.
Waitt, R.B., Mastin, L.G., Miller, T.P., 1995. Ballistic showers during Crater Peak eruptions of Mount Spurr volcano, summer 1992. In: Keith, T.E.C. (Ed.), The 1992 eruptions of Crater Peak vent, Mount Spurr volcano, Alaska. U.S. Geological Survey Bulletin, vol. 2139, pp. 89–106.
Waters, A.C., Fisher, R.V., 1971. Base surges and their deposits: Capelinhos and Taal volcanoes. Journal of Geophysical Research 76, 5596–5614.
Wenrich, K.J., Mascarenas, J.F., 1982. Diatremes of the Hopi Buttes, Arizona: chemical and statistical analysis. U.S. Geological Survey Open-File 82-0740.
White, J.D.L., 1991. Maar–diatreme phreatomagmatism at Hopi Buttes, Navajo Nation (Arizona), USA. Bulletin of Volcanology 53, 239–258.
White, J.D.L., 1996. Impure coolants and interaction dynamics of phreatomagmatic eruptions. Journal of Volcanology and Geothermal Research 74, 155–170.
Williams, H., 1936. Pliocene volcanoes of the Navajo–Hopi country. Bulletin of the Geological Society of America 47, 111–172.
Wohletz, K.H., 1983. Mechanisms of hydrovolcanic pyroclast formation: grain-size, scanning electron microscopy, and experimental studies. Journal of Volcanology and Geothermal Research 17, 31–63.
Wohletz, K.H., 1998. Pyroclastic surges and compressible two-phase flow. In: Freundt, A., Rosi, M. (Eds.), From Magma to Tephra.
Wohletz, K.H., Sheridan, M.F., 1979. A model for pyroclastic surge. Geological Society of America Special Paper 180, 177–194.
Wohletz, K.H., Sheridan, M.F., 1983. Hydrovolcanic explosions II. Evolution of basaltic tuff rings and tuff cones. American Journal of Science 283, 385–413.
Zimanowski, B., Büttner, R., Lorenz, V., Häfele, H., 1997. Fragmentation of basaltic melt in the course of explosive volcanism. Journal of Geophysical Research 102, 803–814.